Optical Properties of Zno Nanoparticles Prepared by Chemical Method Using Poly (VinylAlcohol) (PVA) as Capping Agent

Tapas Kumar Kundu, Nantu Karak , Puspendu Barik , Satyajit Saha

***Abstract*— We report sol-gel synthesis of ZnO nanoparticles in support of poly(vinayl alcohol) (PVA) molecules. PVA molecules offer plenty of active OH groups and a metal ion-polymer complex is formed via a kind of ligand reaction. The particle sizes lie in the range of 23 nm - 43 nm. The Electron paramagnetic resonance (EPR) spectra of the powders are characterized by a broad resonance peak with an average *g*=2.0591 owing to presence of Zn_i^+ defects in the specimens. The nanopowders show an intense violet emission along with the emission in blue and green band. In comparison, ZnO specimens having micron sized grain which are prepared without using PVA do not show any emission with significant intensity. Zn_i^+ defects play a role in improving the optical emission of ZnO nanoparticles prepared by this method. An energy band diagram of nanostructured ZnO specimens explains the photoluminescence results.**

***Index Terms*— Semiconductor Nanocrystal, Optical properties, Luminescence, ZnO**

I. INTRODUCTION

Synthesis and characterization of zinc oxide (ZnO) nanoparticles has found widespread interest during past few years due to their unique electro-optical properties, which can be employed in devices such as ultraviolet (UV) light-emitting diodes (LEDs), blue luminescent devices, UV lasers [1-4]. This system is being widely investigated for better understanding on some fundamental aspects related to the optical, transport and electrical properties of such a wide band gap (3.4 *eV*) semiconductors with large exciton binding energy (60 *meV*). The photoluminescence (PL) spectra of most ZnO nanoparticle samples showed a near band-edge (NBE) UV line accompanied by a strong visible luminescence [5,6]. The most essential aspects of high luminescence efficiencies from ZnO nanoparticles are the surface texture. Some researcher studied a correlation between the visible luminescence and surface properties of colloidal ZnO nanoparticles [7,8]. However, understanding the origin of photoluminescence in ZnO nanoparticles and improving the emission efficiency is still a major challenge for its application in optoelectronic devices.

Surfactant-assisted complex sol–gel process was investigated for synthesizing uniformly distributed ZnO nanoparticles [9-11]. Surface capping by PVA is useful in achieving a higher and relatively steady UV sensitivity in nanostructured ZnO materials. In particular, introduction of ZnO filler into polymeric matrices can modify the optical electrical and mechanical properties. Development of new methods of preparation would allow the particle size, size distribution, crystallinity and morphology to be easily controlled and stabilize the ZnO NPs. There are many reports for the production of ZnO nanoparticles using polymer [12-15]. But in most the cases the polymer was used to activate/deactivate the surface effects of ZnO nanoparticles. Recently, the polymer was used as template to prepare a number of oxide nanoparticles where polymer skeleton eventually limits the growth in a specific shape of the lattice [16-19]. A metal ion-polymer complex forms via a kind of ligand reaction with active OH groups of surfaced PVA molecules. In this paper, we report sol–gel process using $Zn(NO_3)_2.6H_2O$ and NH_4OH assisted by polyvinyl alcohol (PVA) for synthesizing ZnO nanoparticles. The effects of the reaction conditions and sintering on the particle size, crystallinity and morphology were investigated. The reaction between ZnO particles and PVA makes a different structural configuration stable in the system that promotes the optical emission.

II. EXPERIMENTAL

The procedure for the synthesis of ZnO nanoparticles are briefly summarized in Fig. 1. Standard synthetic procedure for the surface-modified ZnO nanoparticles is reported elsewhere [20]. Key step in our method is the introduction of PVA (Mark, $[C_2H_4]_n$, MW 10000) as capping molecules for the preparation of ZnO nanoparticles. To prepare a solution **(A)**, $Zn(NO_3)_2 .6H_2O$ (Mark, M=297.47 gm/mole) was dissolved in distilled deionized water under vigorous stirring at room temperature. Another solution **(B),** PVA in distilled water, was prepared under vigorous stirring at ~ 50 ^oC. Solutions A and B were mixed and NH_4OH solution was added to it dropwise. pH factor of the final solution was maintained at constant value of 12. The white precipitation was filtered and washed with distilled water for several times. Then the precipitations were dried in oven at 90-100 ^oC to obtain white powder. Finally the samples were prepared after burning the PVA through annealing at temperature 500 ^oC (powder I), 700 ^oC (powder II) and 800 ^oC (powder III) for one hour in air. Another sample of ZnO, termed as powder IV, was also prepared without PVA but annealed at 800 ^oC.

Tapas Kumar Kundu, Department of Physics, Visva-Bharati University, Santiniketan (W. B.), India, Ph. No.-+91-9434416277; e-mail: tkkundu1968@yahoo.com

Nantu Karak, Department of Physics, Visva-Bharati University, Santiniketan (W. B.), India, Ph. No.-+91-9933898596; e-mail: ntu.karak@gmail.com

Puspendu Barik, Department of Physics, Visva-Bharati University, Santiniketan (W. B.), India, Ph. No.-+91-9933898596; e-mail: pbarik_mid1983@yahoo.co.in

Satyajit Saha, Department of Physics and Technophysics, Vidyasagar University, Midnapore (W. B.), India; e-mail: sahaphys.vu@gmail.com

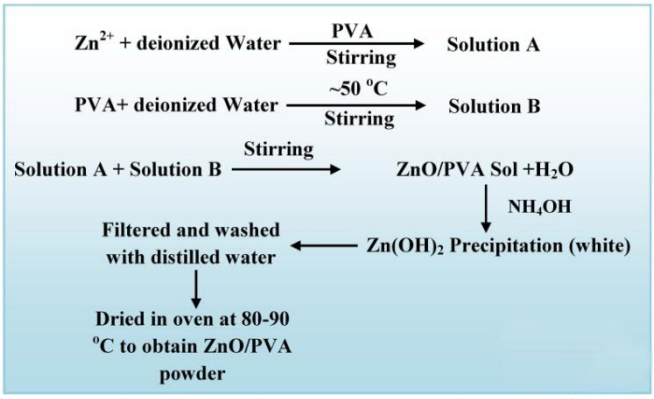

Fig. 1: *The flow diagram for the preparation of PVA modified ZnO nanopowders.*

The crystal structures were checked by using Philips X-ray diffractometer (XRD) (Model PW 1710, $2\theta=3^{o}$-130^{o}, $\Delta 2\theta=0.03^{o}$) with filtered Co-Kα radiation of wavelength λ=0.17889 nm. The average particle sizes were determined from XRD peak widths employing Debye-Scherrer formula. The electron paramagnetic resonance (EPR) spectra were recorded at an X-band frequency (~9.43 GHz) with a Varian Associates spectrometer (model 109). Optical absorptions were recorded by using a Perkin Elmer Lambda 45 UV/VIS spectrophotometer. The excitation and emission spectra were obtained using a Perkin–Elmer (Model-LS55) Luminescence spectrometer in conjunction with a red-sensitive detector (with a gated photomultiplier having modified S5 response), and a pulsed xenon lamp (20kW power with pulse width at half height 510 ms) as excitation source. The data were obtained at a scan rate of 500 nm/min.

III. RESULTS AND DISCUSSIONS

A. *Structural Properties*

Fig. 2(a-d) shows XRD pattern for of powder I, II, III and IV. The XRD patterns are consistent with the spectrum of ZnO powders, and no impurity is found. All XRD diffraction peaks of ZnO powders are shown in a good agreement with hexagonal structure ($P6_{3mc}$) reported in JCPDS File Card No.079-0205. ZnO has a wurtzite structure with the oxygen atoms arranged in a hexagonal close packed lattice and zinc atoms occupying half the tetrahedral sites [21,22].

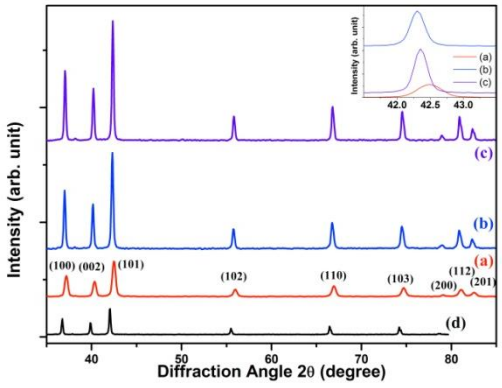

Fig. 2: XRD pattern of (a) powder-I, (b) powder-II, (c) powder-III, and (d) powder-IV. A close-up in the inset compares the shift in (101) peak.

The peak intensity markedly increases with annealing temperature. High annealing temperature provide sufficient energy to crystallites and to orient in proper equilibrium sites and causes an increase in intensity of {101} orientation [23]. From Fig. 2, it was noticed that the full width half maximum (fwhm) of the peaks decreases significantly by using PVA. The average particle size D was calculated using the Debye-Scherrer formula: $D = 0.9\lambda / \beta \cos\theta_b$, where, λ is the x-ray wavelength (0.17889 nm), θ_b is the Bragg diffraction angle, and β is the full width at half maximum. The XRD peaks at 42.48°, 42.29^{o} and 42.34° in Fig. 2 give the ZnO particle diameters of 23 nm, 39 nm and 43 nm, respectively. The XRD broadening of other peaks like (100) and (002) gives the same value of particle diameter. ZnO nanoparticles processed for different annealing temperature have different sizes.

Table I: The values of average particle size (D) calculated from XRD, lattice volume V, lattice number z and density ρ in ZnO nanocrystal

Sample	ZnO					
	D (nm)		V (nm^3)	z	ρ (g/cm^3)	c/a ratio
	XRD	TEM				
Powder I	23	25	0.05355	2	5.0469	1.6105
Powder II	39	42	0.05463	2	4.9471	1.6031
Powder III	43	49	0.05498	2	4.9156	1.6013
Powder IV	76	249	0.04226	2	3.1970	1.8481

The crystallite sizes, lattice volumes, and densities of the specimens are compared in Table I. These data are obtained after a thorough analysis of the XRD patterns. In these specimens, the lattice volume increases with annealing temperature. The microstructure of ZnO nanoparticles have been investigated by TEM image as shown in Fig. 3(a-d). The particle sizes estimated from XRD are close to that measured from TEM as shown in Table I.

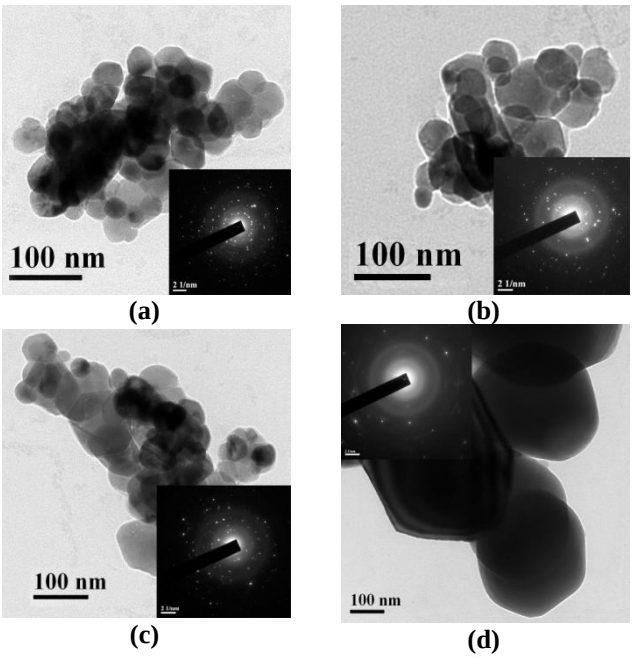

Fig. 3: Transmission Electron Micrograph (TEM) of (a) powder-I (b) powder-II, (c) powder-III, and (d) powder-IV. Insets of the TEM images correspond to the SAED pattern of the ZnO powder.

PVA modified ZnO grains have much lower particle size. PVA molecules offer plenty of active OH groups (free from the H-bonding) to serve as the head groups to adsorb and template the metal cations in a specific pattern. A metal ion-polymer complex forms via a kind of ligand reaction with active OH groups of surfaced PVA molecules. The polymer skeleton eventually limits the growth in such a specific shape of the lattice. Similar templating had been observed and modeled for Cr^{4+} and Zr^{4+} in PVA molecules [16,17]. The diffraction peak positions of hexagonal phase in powder-III

get shifted to higher angle by small value with respect to powder-IV. Inset in Fig. 2 compares {101} peak of h-ZnO at an expanded scale. We use Rietveld Refinement method to analyze the crystal structure. Hence, the data for peak positions and peak widths were taken as per fitted results. Two significant facts are recorded from this representation. First, the peak position (in terms of 2θ) is shifted from 42.02494° (interplanar spacing d_{101} = 0.24945 nm) in powder-IV to 42.35450° (d_{101} = 0.24760 nm) in powder-III. Second, FWHM increases from 0.19667 to 0.236478° as the effect of PVA capping. The analysis by using Rietveld method shows a decrease of c/a with annealing from 1.6105 to 1.6013 and the unit cell lattice volume increases from V = 0.05355 nm^3 to V = 0.05498nm^3. In contrast, the c/a ratio of powder-IV has a value of 1.8481 and lattice volume is V = 0.04226 nm^3. The deviation of the lattice parameters is caused due to presence of various point defects such as zinc antisites, oxygen vacancies, and extended defects, such as threading dislocations. PVA restricts the growth of ZnO particle and the defect states are modified which enhance the optical properties of the materials as explained later.

B. EPR Study

Fig. 4(a) shows the first-order differential electron paramagnetic resonance (EPR) spectra of (a) powder-I (b) powder-II and (c) powder-III. Fig. 4(b) shows comparison between EPR responses from ZnO powder (a) prepared with PVA (b) prepared without PVA, annealed at 800°C for 1 h.

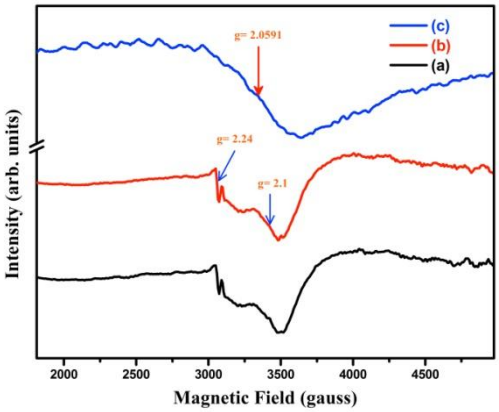

Fig. 4a: X-band (9.429 GHz) EPR traces from (a) powder-I, (b) powder-II, and (c) powder-III.

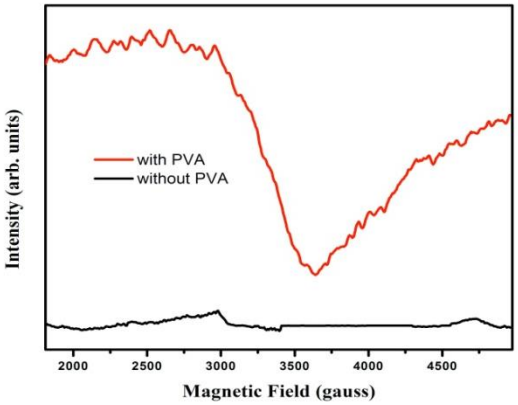

Fig. 4b: Comparison between EPR responses from ZnO powders (a) prepared with PVA (b) prepared without PVA, annealed at 800 ℃ for 1 h.

A broad resonance peak with average g=2.0591 is found in the spectra. Two weak peaks, with g= 2.240 and 2.100 in the background of broad resonance peak, are also observed in powder I and II and these peaks disappeared upon calcining the specimens at a temperature as high as 800^{0}C. EPR responses from microcrystalline ZnO have been reported previously [24]. There can have four types of lattice defects in ZnO. They are (a) V_{zn}, zinc vacancies (b) Zn_i, zinc on interstitial sites (c) O_i, oxygen on interstitial sites and (d) three kinds of oxygen vacancies (V_o^{++}, V_o^{+}, V_o). Singly ionized oxygen vacancy (V_o^{+}) with g = 1.960 and O_i^- with g=1.987 was the dominant paramagnetic defects in most of the cases. The EPR responses from the present set of ZnO powders are due to some kind of defects other than V_o^{+} or O_i^-. Among various defects in ZnO, Zn_i^{+} is also paramagnetic in nature. The EPR signals with g factors in the range 2.0018–2.056 in irradiated single crystals were assigned to Zn vacancies [25,26]. Sometimes it generated an EPR band and a coupling arose between Zn_i^{+} with $V_{Zn,}$ in ZnO nanoparticles [18]. Thus, the EPR responses shown here by the nano-ZnO specimens are due to presence of Zn_i^{+}. The weak signals are generated due to the presence the Zn_i^{+} defects in high energy surface or surface interface in ZnO nanoclusters with smaller grain size as it was explained earlier [18]. No Zn vacancies are detected in larger grained specimens prepared without using capping molecules. This is consistent with the reports that Zn_i^{+} defects in bulk ZnO are not common and it exists in an extremely small amount, of the order of 10^4/cm^3 [24,27].

C. Optical Absorption Study

Fig. 5 shows the optical absorption of (a) powder-I, (b) powder-II and (c) powder-III, and (d) powder-IV. PVA modified ZnO nanopowders show absorption peaks at 383.4 nm, 385.2 nm and 386.2 nm respectively, consistent with the bulk band gap of ZnO [28].

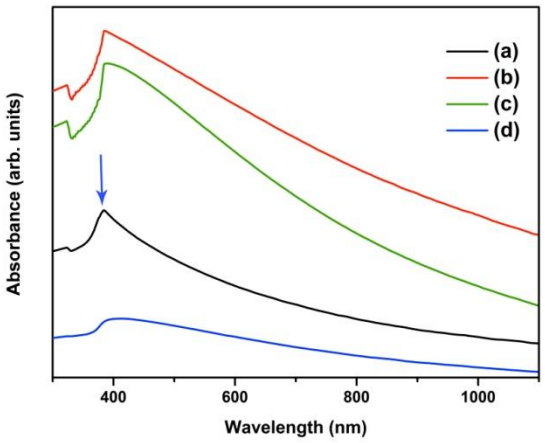

Fig. 5: Optical absorbance curves of (a) powder-I, (b) powder-II, (c) powder-III, and (d) powder-IV.

The absorption spectra demonstrate the absorption peaks around 386 nm (3.23 *eV*) corresponding to the exciton state in the bulk ZnO. Even though these spectra were taken at room temperature, the ZnO nanoparticle samples exhibit salient exciton absorption features due to the relatively large binding energy of the exciton (60 mV). As the annealing temperature is increased, the absorption peak exhibits a progressive redshift. The corresponding redshifts are consistent with the observed variation of the NPs sizes as reported earlier [21]. Since the size of ZnO NCs is nearly 40 nm, that is much more than the exciton Bohr radius in ZnO (r_B=2.34 nm), we observe a small shift of the peak due to quantum confinement effect.

D. Photoluminescence Properties

Fig. 6 shows room temperature photoluminescence spectra from nano ZnO powder samples over wavelength range 350-650 nm on irradiating at wavelength λ_{ex} = 320 nm by a xenon lamp. The excitation energy was chosen from photoluminescence excitation (PLE) spectra of the specimens which show an intense peak at 320 nm. Fig. 6(d) presents the spectrum from micron sized ZnO powder for comparison. The emission spectra are analysed by fitting with multiple Gaussian curves.

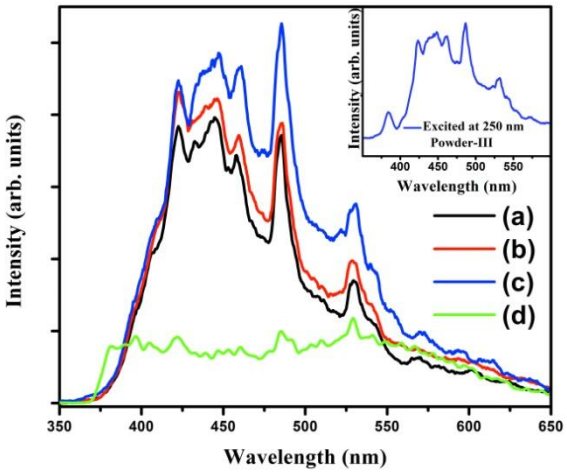

Fig. 6: Emission spectra for (a) powder-I, (b) powder-II, (c) powder-III, and (d) powder-IV. The inset of the figure shows the emission spectra of powder-III (excited at 250 nm).

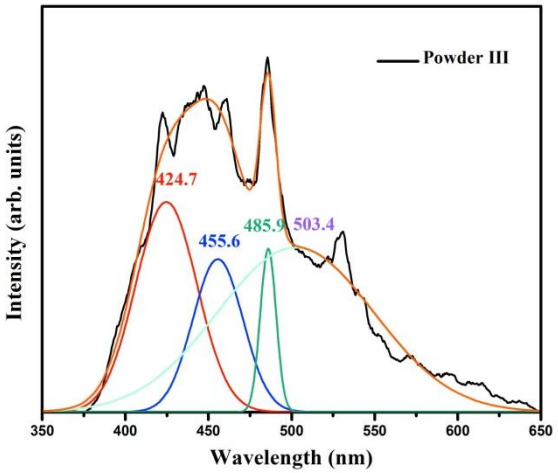

Fig. 7: A deconvolution of the light emission into four bands in ZnO nanopowders prepared with PVA (powder-III).

We are able to fit the PL spectra with four peaks and the fitted profile very closely matches the experimental data. A typical Gaussian fitting of PL characteristic from powder-III is shown in Fig. 7. Peak positions, intensity (I_p) and fwhm of the curves are summarized in Table II. The nanopowders show an intense violet emission along with the emission in blue and green band. Average position of the most intense peak lies in the violet band in the range 417-424 nm. Blue emission band occurs in the range (a) 447-455 nm (Band-I) (b) 485-486 nm (Band-II). A green emission band occurs at 500-504 nm. Like other reports [6,21,29], we draw a probable band diagram showing the mechanism behind different emission bands.

In the photoluminescence (PL) spectra of ZnO, typically there are emission bands in the UV and visible regions. The UV peak is usually considered as the characteristic emission of ZnO and attributed to the band edge emission or the exciton transition. But there were many reports that showed the characteristic emission of ZnO was absent in their luminescence spectra [29,30]. Generally the UV emission in ZnO disappears in two cases. First, if the excitation energy is considerably lower that its band gap energy [29] and second, if the intensity of visible emission is much higher due to increased defect density [31,32]. In our case the UV emission does not appear as the excitation wavelength is 325 nm. If we excite the specimens at a wavelength of 300 nm or less there is UV emission as shown in the inset of Fig. 6.

Table II: Band positions, bandwidths, and relative intensities in individual bands after deconvolution of the observed light emission in ZnO nanocrystals

Powder No.	Position (nm)	I_p	fwhm (nm)
Powder I	417.9	39.83	31.65
	447.5	49.16	36.90
	485.5	36.79	8.56
	500.9	27.31	95.35
Powder II	422.8	56.91	33.64
	453.5	43.15	33.44
	485.9	37.98	9.03
	502.7	30.58	98.66
Powder III	424.7	60.22	36.94
	455.6	42.88	30.20
	485.9	46.84	10.09
	503.4	47.20	100.07

The observed emission in the ZnO nanocrystallites is described with a band diagram as shown in Fig. 8. The presence of different types of defects and their effect are considered in this model. The first principle study shows that the Zn_{3d} electron strongly interacts with the O_{2p} electron in ZnO [29]. Oxygen has tightly bound 2p electrons and Zn has tightly bound 3d electrons, which sense the nuclear attraction efficiently. As shown in the Fig. 8a, Violet luminescence at ~417-424 nm (2.92-3.00 *eV*) is attributed to the transition from conduction band to the deep holes trapped levels like V_{Zn} [21,33].

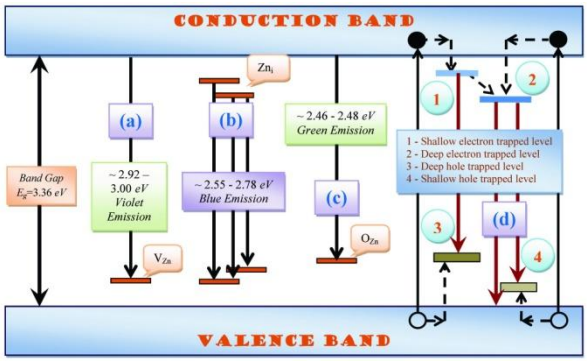

Fig. 8: Schematic view of the energy band diagram proposed for ZnO nanopowders.

The energy interval ~2.73-2.78 *eV* between acceptor states and donor states supports the emission at a wavelength of 447-455 nm (Blue Band-I) as shown in the Fig. 8(b). The intensity of the blue (band-I) luminescence decreases with annealing temperature. Zn_i are responsible for these emissions which are also supported by the EPR results. The intensity of this band decreases as the concentration of Zn_i in the powders was diffused with post annealing process of the sample [32]. The blue (Band-II) emission can be ascribed to the direct recombination of conduction electron in the Zn_{3d} band and a hole in the O_{2p} valance band. This emission at

about 485.5–485.9 nm (2.55-2.56 *eV*) for three samples may have originated from the transition due to the oxygen antisite vacancy defect O_{Zn} as shown in the Fig. 8(c) [33,36].

Fig. 8(d) shows the typical process for green emission at 500 -504 nm (2.46-2.48 *eV*): the mechanism of the transition (1) from near conduction band edge to deep acceptor level and (2) from deep donor level to valence band. The recombination of a shallowly trapped electron with a deeply trapped hole in a V_o^{++} center causes visible emission [37]. The green luminescence was observed in different ZnO samples prepared with a variety of growth techniques. In some cases, the presence of foreign element like Cu was suggested for the emission [38]. Native defects have also been suggested as a potential source. Researchers hypothesized that interstitial Zn and oxygen are the centers responsible for green luminescence [39-42]. Earlier studies suggested a correlation between green luminescence and the ZnO-*B* electron paramagnetic resonance (EPR) signal (g = 1.96), attributed to oxygen vacancies in reduced ZnO [35]. Some researcher found that there is no simple relationship between the intensity of g=1.96 EPR signal and the visible PL; the green PL is observed for the samples which do not show EPR line at g=1.96, and they conclude that the explanation for the green luminescence involves multiple defects and/or defect complexes and the major part of the visible emission originates from the defect centers at the surface of the nanoparticles [43]. Here the emission of the green luminescence involves multiple defects and/or defect complexes and the major part of the visible emission originate from the defect centers at the surface of the nanoparticles. The shift of the emission with the increase of annealing temperature is believed to originate from the residual stress due to the lattice distortion. A decrease in lattice constant 'c' was observed in the annealed powder which results in decrease of the band gap.

IV. CONCLUSION

ZnO nanoparticles are prepared by sol–gel process in support of polyvinyl alcohol (PVA) molecules. The particle sizes lie in the range of 23 nm - 43 nm. PVA molecules offer plenty of active OH groups to adsorb the metal cations in a specific pattern. A metal ion-polymer complex forms via a kind of ligand reaction with active OH groups of surfaced PVA molecules. The polymer skeleton eventually limits the growth in a specific shape of the lattice. The analysis by using Rietveld method shows an increase of unit cell lattice volume of nano-ZnO from V = 0.04226 nm^3 (for bulk) to V = 0.05355 nm^3. The deviation of the lattice parameters is caused due to presence of various point defects such as zinc antisites, oxygen vacancies, and extended defects. The Electron paramagnetic resonance (EPR) spectra of the powders are characterized by a broad resonance peak with average g=2.0591 owing to presence of Zn_i^+ defects in the specimens. Such defects are not observable in other ZnO specimens having micron sized grain which are prepared without using PVA.

The powders show intense violet emission (peak at ~417-424 nm) along with the emission in blue and green band. In comparison, ZnO specimens having micron sized grain which are prepared without using PVA do not show any emission with significant intensity. A correlation between the PL band and EPR band intensity is found for blue luminescence peak at 447-455 nm. The green emission originates mainly from the heterogeneity of the surface traps, changing deep level defect states and particle diameter. An energy band diagram of nanostructured ZnO specimens explains the photoluminescence results.

References

[1] L. Chopra, S. Major, and D.K. Panday, *Transparent conductors—A status review*, *Thin Solid Films* 102, 1983, pp. 1-46.

[2] S. Bose and A.K. Barua, *The role of ZnO: Al films in the performance of amorphous-silicon based tandem solar cells*, *J. Phys. D: Appl. Phys*. 32, 1999, pp. 213-218.

[3] H. Kim, C.M. Gilmore, J.S. Horwitz, A. Pique, H. Murata, G.P. Kushto, R. Schlaf, Z.H. Kafafi, and D.B. Chrisey, *Transparent conducting aluminum-doped zinc oxide thin films for organic light-emitting devices*, *Appl. Phys. Lett*. 76, 2000, pp. 259-261.

[4] H.M. Cheng, H.C. Hsu, S.L. Chen, W.T. Wu, C.C. Kao, L.J. Lin, and W.F. Hsieh, *Efficient UV photoluminescence from monodispersed secondary ZnO colloidal spheres synthesized by sol–gel method*, *J. Cryst. Growth* 277, 2005, pp. 192-199.

[5] L. Guo, S. Yanga, C. Yang, P. Yu, J. Wang, W.Ge, and G.K.L. Wong, *Highly monodisperse polymer-capped ZnO nanoparticles: Preparation and optical properties*, *Appl. Phys. Lett*. 76, 2000, pp. 2901-2903.

[6] B. Lin, Z. Fu, Y. Jia, *Green luminescent center in undoped zinc oxide films deposited on silicon substrates*, *Appl. Phys. Lett*. 79, 2001, pp. 943-945.

[7] S. Sakohara, M. Ishida, and M.A. Anderson, *Visible Luminescence and Surface Properties of Nanosized ZnO Colloids Prepared by Hydrolyzing Zinc Acetate*, *J. Phys. Chem. B* 102, 1998, pp. 10169-10175.

[8] S. Monticone, R. Tufeu, and A.V. Kanaev, *Complex Nature of the UV and Visible Fluorescence of Colloidal ZnO Nanoparticles*, *J. Phys. Chem. B* 102, 1998, pp. 2854-2862.

[9] J. Lee, D. Bhattacharyya, A.J. Easteal, and J.B. Metson, *Properties of nano-ZnO/poly(vinyl alcohol)/poly(ethylene oxide) composite thin film*, *Curr. Appl. Phys*. 8, 2008, pp. 42-47.

[10] X.M. Sui, C.L. Shao, and Y.C. Liu, *White-light emission of polyvinyl alcohol/ZnO hybrid nanofibers prepared by electrospinning*, *Appl. Phys. Lett.* 87, 2005, pp. 113115-113117.

[11] M. Xiong, G. Gu, B. You, and L. Wu, *Preparation and Characterization of Poly(styrene butylacrylate) Latex/Nano-ZnO Nanocomposites*, *J. Appl. Polym. Sci.* 90, 2003, pp. 1923-1931.

[12] Y. Wang, C. Ma, X. Sun, and H. Li, *Preparation of nanocrystalline metal oxide powders with the surfactant-mediated method*, *Inorg. Chem. Commun*. 5, 2002, pp. 751–755.

[13] Y.L. Zhang, Y. Yang, J.H. Zhao, R.Q. Tan, P. Cui, W.J. Song, *Preparation of ZnO nanoparticles by a surfactant-assisted complex sol–gel method using zinc nitrate*, *J. Sol-Gel Sci. Technol*. 51, 2009, pp. 198–203.

[14] A. Bera and D. Basak, *Effect of Surface Capping with Poly(vinyl alcohol) on the Photocarrier Relaxation of ZnO Nanowires*, ACS *Appl. Mat. Interfaces* 1, 2009, pp. 2066-2070.

[15] H. Zhang, D. Yang, D. Li, X. Ma, S. Li, and D. Que, *Controllable Growth of ZnO Microcrystals by a Capping-Molecule-Assisted Hydrothermal Process*, *Cryst. Growth Des.* , 2005, pp. 547-550.

[16] S. Biswas and S. Ram, *Morphology and stability in a half-metallic ferromagnetic CrO_2 compound of nanoparticles synthesized via a polymer precursor*, *Chem. Phys*. 306, 2004, pp. 163-169.

[17] S. Ram, *Synthesis and structural and optical properties of metastable ZrO_2 nanoparticles with intergranular Cr^{3+}/Cr^{4+} doping and grain surface modification*, *J. Mater. Sci*. 35, 2003, pp. 643-655.

[18] S. Ram and T.K. Kundu, *Synthesis and unusual electron paramagnetic resonance spectrum of ZnO semiconductor in a metastable structure of nanoclusters*, *J Nanosci. Nanotechnol*. 4, 2004, pp. 1076-1080.

[19] A. Jana, T.K. Kundu, *Microstructure and dielectric characteristics of Ni ion doped $BaTiO_3$ nanoparticles*, *Mater. Lett*. 61, 2007, pp. 1544–1548.

[20] L. Spanhel and M.A. Anderson, *Semiconductor Clusters in the Sol-Gel Process: Quantized Aggregation, Gelation, and Crystal Growth in Concentrated ZnO Colloids*, *J. Am. Chem. Soc*. 113, 1991, pp. 2826-2833.

[21] L. Irimpan, V.P.N. Nampoori, P. Radhakrishnan, A. Deepthy, and B. Krishnan, *Size dependent fluorescence spectroscopy of nanocolloids of ZnO*, *J. Appl. Phys.* 102, 2007, pp. 063524-063529.

[22] V.A.L. Roy, A.B. Djurisic, W.K. Chan, J. Gao, H.F. Lui, and C. Surya, *Luminescent and structural properties of ZnO nanorods prepared under different conditions*, *Appl. Phys. Lett*. 83, 2003, pp. 141-143.

[23] P. Sagar, P.K. Shishodia, R.M. Mehra, H. Okada, A. Wakahara, and A. Yoshida, *Photoluminescence and absorption in sol–gel-derived ZnO films*, *J. Lumin*. 126, 2007, pp. 800-806.
[24] B. Yu, C. Zhu, F. Gan, and Y. Huang, *Electron spin resonance properties of ZnO microcrystallites*, *Mater. Lett*. 33, 1998, pp. 247-250.
[25] A.L. Taylor, G. Filipovich, and G.K. Lindeberg, *Electron paramagnetic resonance associated with Zn vacancies in neutron-irradiated ZnO*, *Solid State Commun*. 8, 1970, pp. 1359-1361.
[26] D. Galland and A. Herve, *ESR spectra of the zinc vacancy in ZnO*, *Phys. Lett. A* 33, 1970, pp. 1-2.
[27] K. Hoffmann and D. Hahn, *Electron Spin Resonance of Lattice Defects in Zinc Oxide*, *Phys. Status Solidi A* 24, 1974, pp. 637-648.
[28] K.G. Kanade, B.B. Kale, R.C. Aiyer, and B.K. Das, *Effect of solvents on the synthesis of nano-size zinc oxide and its properties*, *Mater. Res. Bull*. 41, 2006, pp. 590-600.
[29] K. Vanheusden, W.L. Warren, C.H. Seager, D.R. Tallant, J.A. Voigt, and B.E. Gnade *Mechanisms behind green photoluminescence in ZnO phosphor powders*, *J. Appl. Phys*. 79, 1996, pp. 7983-7990.
[30] W.C. Zhang, X.L. Wu, H.T. Chen, J. Zhu, and G.S. Huang, *Excitation wavelength dependence of the visible photoluminescence from amorphous ZnO granular films*, *J. Appl. Phys*. 103, 2008, pp. 093718-093722.
[31] C.H. Hung and W.T. Whang, *Effect of surface stabilization of nanoparticles on luminescent characteristics in ZnO/poly(hydroxyethyl methacrylate) nanohybrid films*, *J. Mater. Chem.* 15, 2005, pp. 267–274.
[32] H. Zeng, W. Cai, J. Hu, G. Duan, P. Liu, and Y. Li, *Violet photoluminescence from shell layer of Zn/ZnO core-shell nanoparticles induced by laser ablation*, *Appl. Phys. Lett*. 88, 2006, pp. 171910-171912.
[33] P. Schroer, P. Kriiger and J. Pollmann, *First-principle calculation of the electronic structure of the wurtzite semiconductors ZnO and ZnS*, *Phys. Rev. B* 47, 1993, pp. 6971-6980.
[34] Z. Fang, Y. Wang, D. Xu, Y. Tan, and X. Liu, *Blue luminescent center in ZnO films deposited on silicon substrates*, *Opt. Mater*. 26, 2004, pp. 239-242.
[35] P.H. Kasai, *Electron Spin Resonance Studies of Donors and Acceptors in ZnO*, *Phys. Rev*. 130, 1963, pp. 989-995.
[36] R.B. Kale, Y.J. Hsu, Y.F. Lin, and S.Y. Lu, *Synthesis of stoichiometric flowerlike ZnO nanorods with hundred per cent morphological yield*, *Solid State Commun*. 142, 2007, pp. 302-305.
[37] A. Van Dijken, E.A. Meulenkamp, D. Vanmaekelbergh, and A. Meijerink, *The Kinetics of the Radiative and Nonradiative Processes in Nanocrystalline ZnO Particles upon Photoexcitation*, *J. Phys. Chem. B* 104, 2000, pp. 1715-1723.
[38] K.C. Mishra, P.C. Schmidt, K.H. Johnson, B.G. DeBoer, J.K. Berkowitz, and E.A. Dale, *Bands versus bonds in electronic-structure theory of metal oxides: Application to luminescence of copper in zinc oxide*, *Phys. Rev. B* 42, 1990, pp. 1423-1430.
[39] D.C. Reynolds, D. C. Look, B. Jogai and H. Morkoç, *Similarities in the bandedge and deep-centre photoluminescence mechanisms of ZnO and GaN*, *Solid State Commun*. 101, 1997, pp. 643-646.
[40] A.F. Kohan, G. Ceder, D. Morgan and G. Chris Van de Walle, *First-principles study of native point defects in ZnO*, *Phys. Rev. B* 61, 2000, pp. 15019-15027.
[41] F.A. Kroger and H.J. Vink, *The Origin of the Fluorescence in Self Activated ZnS, CdS, and ZnO*, *J. Chem. Phys.* 22, 1954, pp. 250-252.
[42] M. Liu, A.H. Kitai and P. Mascher, *Point defects and luminescence centres in zinc oxide and zinc oxide doped with manganese*, *J. Lumin*. 54, 1992, pp. 35-42.
[43] D. Li, Y.H. Leung, A.B. Djurisic, Z.T. Liu, M.H. Xie, S.L. Shi, S.J. Xu, and W.K. Chan, *Different origins of visible luminescence in ZnO nanostructures fabricated by the chemical and evaporation methods*, *Appl. Phys. Lett.* 85, 2004, pp. 1601-1603.